

**CT Based Three-Dimensional Measurement of
Adult Orbit in Hospital Universiti Sains
Malaysia**

By

DR. LEE CHEE KONG

**DISSERTATION SUBMITTED IN PARTIAL
FULFILLMENT OF THE REQUIREMENTS FOR
THE DEGREE OF MASTER OF MEDICINE
RADIOLOGY**



**SCHOOL OF MEDICAL SCIENCES
UNIVERSITI SAINS MALAYSIA
2015**

**CT Based Three-Dimensional Measurement of
Adult Orbit in Hospital Universiti Sains
Malaysia**

BY:

DR. LEE CHEE KONG

**Dissertation Submitted in Partial
Fulfillment of The Requirements For
The Degree of Master of Medicine
Radiology**

UNIVERSITI SAINS MALAYSIA

2015

Supervisors:

**Assoc. Prof Dr. Meera Mohaideen Abdul
Kareem**

To my wife, Alicia Chong,

Her love and patience has helped to unlock the fullness in my life. Her perpetual support has helped to turn chaos to order, confusion to clarity and denial into acceptance. Without her, this masterpiece would not have been completed.

To my only son, Lee Guan Yit,

His presence has turned every living minute into a spiritual experience of love, grace and gratitude. I am really thankful for him being in my life.

To my family members,

They helped me to make sense of my past, bring peace for today and create a vision for tomorrow.

ACKNOWLEDGEMENT

Thank you is the least I can say to all the individuals to show my appreciation for everything that they have done for me throughout the period of my dissertation project. Sincerest appreciation to my supervisor, Associate Professor Dr. Meera Mohaideen Abdul Kareem (Lecturer and Radiologist, Department of Radiology, School of Medical Sciences, Universiti Sains Malaysia, Kubang Kerian, Kelantan) for his guidance and supervision. His exemplary knowledge and vast rich experience in the research field of radiology has greatly enlightened my myopic view. The kindness and patience that he has shown to me during this whole period has been a pillar of support for me.

I would also like to take this opportunity to convey my deepest gratitude to the following individuals for their support of this dissertation project. Their patience, help and encouragement has helped to turn my dream of this dissertation into a reality. Sincerest thanks to:

- **Dr. Nik Munirah bt Nik Mahdi**, Head of Department, Department of Radiology at Hospital Universiti Sains Malaysia.
- **Dr. Mohd Shaffie b Baba**, Head of Department, Department of Radiology at Hospital Raja Permaisuri Bainun, Ipoh, Perak.
- **Dr. Nurashikin Jamaluddin**, Registra of Radiology, Department of Radiology at Hospital Universiti Sains Malaysia.
- **Dr. Prahalad Ramanathan**, Registra of Radiology, Department of Radiology at Hospital Universiti Sains Malaysia.
- **Dr. Suraya Hanim**, 3rd year Resident of Radiology, Department of Radiology at Hospital Universiti Sains Malaysia.
- **Dr. Fauziah**, Radiologist Department of Radiology at Hospital Raja Permaisuri Bainun, Ipoh, Perak.

- **Dr. Rozita**, Radiologist Department of Radiology at Hospital Raja Permaisuri Bainun, Ipoh, Perak.
- **Dr. Sarimah Abdullah**, Unit of Biostatistics and Research Methodology, School of Medical Sciences, Universiti Sains Malaysia, Kubang Kerian, Kelantan.
- **Professor Dr. Syed Hatim Noor@Nyi Nyi Naing**, Unit of Biostatistics and Research Methodology, School of Medical Sciences, Universiti Sains Malaysia, Kubang Kerian, Kelantan.
- All lecturers/radiologists, Department of Radiology, School of Medical Sciences, Universiti Sains Malaysia, Kubang Kerian, Kelantan.
- Hospital Raja Permaisuri Bainun Radiographers.
- Hospital University Sains Malaysia Radiographers.
- **Dr. Alex Lee Fook Seng**, Radiologist Hospital Teluk Intan
- **Dr. Julian Ong Joo Lian**, Radiologist Hospital Sibul
- **Dr. Chow Kok Soon**, Radiologist Hospital Johor Bharu

TABLE OF CONTENT

ACKNOWLEDGEMENT	ii
TABLE OF CONTENT	iv
LIST OF FIGURES	vii
LIST OF TABLES	xii
LIST OF ABBREVIATIONS, SYMBOLS AND ACRONYMS	xv
ABSTRACT	xvi
CHAPTER 1 INTRODUCTION	1
CHAPTER 2 LITERATURE REVIEW	6
2.1 Introduction to CT Scan.....	6
2.2 Reconstruction Algorithm	7
2.3 Three Dimensional (3D) Surface Reconstruction Imaging.....	8
2.4 CT Scan Of The Orbit And Brain	9
2.5 Anatomy of the Orbit.....	10
2.6 Orbital Angle, Fissures and Optic Canal.....	12
2.7 Supraorbital Foramina and Infraorbital Foramina	13
2.8 Extraocular Muscle	14
2.9 Skull Changes with Age.....	15
CHAPTER 3 OBJECTIVE.....	18
3.1 General Objectives	18
3.2 Specific Objectives	18
CHAPTER 4 METHODOLOGY	20
4.1 Study Design	20
4.2 Research Questions	20
4.3 Sampling Method.....	20
4.4 Sample Size	20
4.4.1 Sample Size for Objective.....	21
4.5 Inclusion criteria	21
4.6 Exclusion criteria	21
4.7 Methods.....	22
4.7.1 CT Examination	23

4.7.2	CT Scan Protocol.....	23
4.7.3	Image Analysis.....	24
4.8	Flow Chart for Data Collection.....	29
4.9	Statistical Analysis.....	30
CHAPTER 5	RESULTS	32
5.1	Demography Data	32
5.2	Correlation and Regression of Normalized Height, Width and Perimeter of Both Orbits.....	33
5.2.1	Comparison of Normalized Height of Left and Right Orbit	33
5.2.2	Comparison of Normalized Width of Left and Right Orbit.....	35
5.2.3	Comparison of Normalized Perimeter of Left and Right Orbit	38
5.3	Measurement of Normalized Height, Width and Perimeter of Both Orbits with Race	40
5.3.1	Measurement of Normalized Height of Left Orbit with Race	40
5.3.2	Measurement of Normalized Right Height of Orbit with Race	42
5.3.3	Measurement of Normalized Width of Left Orbit with Race.....	44
5.3.4	Measurement of Normalized Width of Right Orbit with Race	46
5.3.5	Measurement of Normalized Perimeter of Left Orbit with Race	48
5.3.6	Measurement of Normalized Perimeter of Right Orbit with Race	50
5.4	Measurement of Normalized Height, Width and Perimeter of Both Orbits with Gender.....	53
5.4.1	Measurement of Normalized Height of Left Orbit with Gender.....	53
5.4.2	Measurement of Normalized Height of Right Orbit with Gender.....	55
5.4.3	Measurement of Normalized Width of Left Orbit with Gender	57
5.4.4	Measurement of Normalized Width of Right Orbit with Gender.....	59
5.4.5	Measurement of Normalized Perimeter of Left Orbit with Gender.....	61
5.4.6	Measurement of Normalized Perimeter of Right Orbit with Gender.....	63
5.5	Measurement of Normalized Height, Width and Perimeter of Both Orbits with Age	65
5.5.1	Measurement of Normalized Height of Left Orbit with Age	65
5.5.2	Measurement of Normalized Height of Right Orbit with Age	70
5.5.3	Measurement of Normalized Width of Left Orbit with Age.....	74

5.5.4	Measurement of Normalized Width of Right Orbit with Age	78
5.5.5	Measurement of Normalized Perimeter of Left Orbit with Age	82
5.5.6	Measurement of Normalized Perimeter of Right Orbit with Age	86
CHAPTER 6 DISCUSSION.....		92
6.1	Demographic.....	92
6.2	Comparison of the Normalized Width, Height and Perimeter of Left and Right Orbit	93
6.3	Comparison of the Normalized Width, Height and Perimeter of Both Orbits with Race.....	96
6.4	Comparison of the Normalized Orbital Width, Height and Perimeter of Both Orbits with Gender.....	96
6.5	Comparison of the Normalized Orbital Width, Height and Perimeter of Both Orbits with Age Group	97
6.6	Measurement using 3-Dimensional CT scan.....	97
CHAPTER 7 CONCLUSION.....		100
CHAPTER 8 LIMITATION		101
CHAPTER 9 RECOMMENDATION.....		102
CHAPTER 10 REFERENCES		103
APPENDIX A: HUMAN ETHICAL APPROVAL		107
APPENDIX B: TABLE OF RAW DATA COLLECTION		116
APPENDIX C: CALCULATION OF PATIENT DATA		131
APPENDIX D: CENSUS OF KELANTAN POPULATION		134
APPENDIX E: GANTT CHART		135

LIST OF FIGURES

Figure 2.1	Osteology of the orbit (Balasubramanian, 2006).....	11
Figure 2.2	Schematic representation of the osteology of the orbit from a frontal projection (John, 2011)	11
Figure 2.3	Orbital fissure and optic canal (John, 2011).....	13
Figure 2.4	Anatomy of the extraocular muscle (AAPOS, 2015)	15
Figure 2.5	Anatomy of extraocular muscle on CT (Kolb, 2015).....	15
Figure 4.1	Readjustment of the CT brain images prior to 3D reconstruction (images taken from our own workstation).....	25
Figure 4.2	3D reconstructed image of the coronal view of the CT brain with the 11 vertical lines arranged equally distanced. (Images captured from our own workstation)	26
Figure 4.3	Measurement of the perimeter of the orbital rim. (Image obtained from our own workstation)	27
Figure 4.4	Measurement of the orbital rim height and width. (Images taken from our own workstation)	28
Figure 5.1	Scatter plot with a regression line between the height of the left and right orbit among the participants (n=126).....	33
Figure 5.2	Histogram of distribution of left height among the participants (n=126)	34
Figure 5.3	Histogram of distribution of right height among the participants (n=126)	34
Figure 5.4	Scatter plot with a regression line between the left width and right width among the participants (n=126)	35
Figure 5.5:	Histogram of distribution of width of left orbit among the participants (n=126)	36
Figure 5.6:	Histogram of distribution of width of right orbit among the participants (n=126)	37
Figure 5.7	Scatter plot with a regression line between the perimeter of left and right orbit among the participants (n=126).....	38
Figure 5.8	Histogram of distribution of perimeter of left orbit among the participants (n=126)	39
Figure 5.9	Histogram of distribution of perimeter of right orbit among the participants (n=126)	39

Figure 5.10	Histogram of distribution of height of left orbit among the Malay participants (n=113).....	41
Figure 5.11	Histogram of distribution of height of left orbit among the non-Malay participants (n=13).....	41
Figure 5.12	Histogram of distribution of height of the right orbit among the Malay participants (n=113).....	43
Figure 5.13	Histogram of distribution of height of the right orbit among the non-Malay participants (n=13).....	43
Figure 5.14	Histogram of distribution of width of the left orbit among the Malay participants (n=113).....	45
Figure 5.15	Histogram of distribution of width of the left orbit among the non-Malay participants (n=113).....	45
Figure 5.16	Histogram of distribution of width of the right orbit among the Malay participants (n=113).....	47
Figure 5.17	Histogram of distribution of width of the right orbit among the non-Malay participants (n=13).....	47
Figure 5.18	Histogram of distribution of perimeter of left orbit among the Malay participants (n=113).....	49
Figure 5.19	Histogram of distribution of perimeter of left orbit among the non-Malay participants (n=13).....	49
Figure 5.20	Histogram of distribution of perimeter of the right orbit among the Malay participants (n=113).....	51
Figure 5.21	Histogram of distribution of perimeter of the right orbit among the non-Malay participants (n=113).....	52
Figure 5.22	Histogram of distribution of height of the left orbit among the male participants (n=68)	54
Figure 5.23	Histogram of distribution of height of the left orbit among the female participants (n=58)	54
Figure 5.24	Histogram of distribution of height of the right orbit among the male participants (n=68)	56
Figure 5.25	Histogram of distribution of height of the right orbit among the female participants (n=58)	56
Figure 5.26	Histogram of distribution of width of the left orbit among the male participants (n=68)	58

Figure 5.27	Histogram of distribution of width of the left orbit among the female participants (n=58)	58
Figure 5.28	Histogram of distribution of width of the right orbit among the male participants (n=68)	60
Figure 5.29	Histogram of distribution of width of the right orbit among the female participants (n=58)	60
Figure 5.30	Histogram of distribution of perimeter of the left orbit among the male participants (n=68)	62
Figure 5.31	Histogram of distribution of perimeter of the left orbit among the female participants (n=58).....	62
Figure 5.32	Histogram of distribution of perimeter of the right orbit among the male participants (n=68)	64
Figure 5.33	Histogram of distribution of perimeter of the right orbit among the female participants (n=58).....	64
Figure 5.34	Histogram of distribution of height of the left orbit among the participants less than 21 years old (n=11)	66
Figure 5.35	Histogram of distribution of height of the left orbit among the participants between 21-30 years old (n=5)	67
Figure 5.36	Histogram of distribution of height of the left orbit among the participants between 31-40 years old (n=19)	67
Figure 5.37	Histogram of distribution of height of the left orbit among the participants between 41-50 years old (n=19)	68
Figure 5.38	Histogram of distribution of height of the left orbit among the participants between 51-60 years old (n=30)	68
Figure 5.39	Histogram of distribution of height of the left orbit among the participants more than 60 years old (n=42).....	69
Figure 5.40	Histogram of distribution of height of the right orbit among the participants less than 21 years old (n=11)	71
Figure 5.41	Histogram of distribution of height of the right orbit among the participants between 21-30 years old (n=5)	71
Figure 5.42	Histogram of distribution of height of the right orbit among the participants between 31-40 years old (n=19)	72
Figure 5.43	Histogram of distribution of height of the right orbit among the participants between 41-50 years old (n=19)	72

Figure 5.44	Histogram of distribution of height of the right orbit among the participants between 51-60 years old (n=30)	73
Figure 5.45	Histogram of distribution of height of the right orbit among the participants more than 60 years old (n=42).....	73
Figure 5.46	Histogram of distribution of width of the left orbit among the participants less than 21 years old (n=11)	75
Figure 5.47	Histogram of distribution of width of the left orbit among the participants between 21-30 years old (n=5)	75
Figure 5.48	Histogram of distribution of width of the left orbit among the participants between 31-40 years old (n=19)	76
Figure 5.49	Histogram of distribution of width of the left orbit among the participants between 41-50 years old (n=19)	76
Figure 5.50	Histogram of distribution of width of the left orbit among the participants between 51-60 years old (n=30)	77
Figure 5.51	Histogram of distribution of width of the left orbit among the participants more than 60 years old (n=42).....	77
Figure 5.52	Histogram of distribution of width of the right orbit among the participants less than 21 years old (n=11)	79
Figure 5.53	Histogram of distribution of width of the right orbit among the participants between 21-30 years old (n=5)	79
Figure 5.54	Histogram of distribution of width of the right orbit among the participants between 31-40 years old (n=19)	80
Figure 5.55	Histogram of distribution of width of the right orbit among the participants between 41-50 years old (n=19)	80
Figure 5.56	Histogram of distribution of width of the right orbit among the participants between 51-60 years old (n=30)	81
Figure 5.57	Histogram of distribution of width of the right orbit among the participants more than 60 years old (n=42).....	81
Figure 5.58	Histogram of distribution of perimeter of the left orbit among the participants less than 21 years old (n=11).....	83
Figure 5.59	Histogram of distribution of perimeter of the left orbit among the participants between 21-30 years old (n=5)	83
Figure 5.60	Histogram of distribution of perimeter of the left orbit among the participants between 31-40 years old (n=19)	84

Figure 5.61	Histogram of distribution of perimeter of the left orbit among the participants between 41-50 years old (n=19)	84
Figure 5.62	Histogram of distribution of perimeter of the left orbit among the participants between 51-60 years old (n=30)	85
Figure 5.63	Histogram of distribution of perimeter of the left orbit among the participants more than 60 years old (n=42).....	85
Figure 5.64	Histogram of distribution of perimeter of the right orbit among the participants less than 21 years old (n=11).....	87
Figure 5.65	Histogram of distribution of perimeter of the right orbit among the participants between 21-30 years old (n=5)	88
Figure 5.66	Histogram of distribution of perimeter of the right orbit among the participants between 31-40 years old (n=19)	88
Figure 5.67	Histogram of distribution of perimeter of the right orbit among the participants between 41-50 years old (n=19)	89
Figure 5.68	Histogram of distribution of perimeter of the right orbit among the participants between 51-60 years old (n=30)	89
Figure 5.69	Histogram of distribution of perimeter of the right orbit among the participants more than 60 years old (n=42).....	90

LIST OF TABLES

Table 5:1	Frequency and percentage of the demographic characteristics of the participants (n = 126)	32
Table 5:2	Relationship between height of the left and right orbit among the participants (n=126)	34
Table 5:3	Correlation between height of left and right orbit among the participants (n=126)	35
Table 5:4	Relationship between the width of left and right orbit among the participants (n=126)	36
Table 5:5	Correlation between width of left and right orbit among the participants (n=126)	37
Table 5:6	Relationship between perimeter of the left and right orbit among the participants (n=126)	38
Table 5:7	Correlation between width of left and right orbit among the participants (n=126)	40
Table 5:8	Mean and standard deviation of the height of the left orbit for both races (n=126).....	40
Table 5:9	Comparison of height of left orbit between the Malay and non-Malay (n=126).....	42
Table 5:10	Mean and standard deviation of the height of the right orbit for both races (n=126).....	42
Table 5:11	Comparison of height of right orbit between the Malay and non-Malay (n=126).....	44
Table 5:12	Mean and standard deviation of the width of the left orbit for both races (n=126).....	44
Table 5:13	Comparison of width of the left orbit between the Malay and non-Malay (n=126).....	46
Table 5:14	Mean and standard deviation of the width of the right orbit for both races (n=126).....	46
Table 5:15	Comparison of width of right orbit between the Malay and non-Malay (n=126).....	48
Table 5:16	Mean and standard deviation of the perimeter of the left orbit for both races (n=126).....	48

Table 5:17	Comparison of perimeter of left orbit between the Malay and non-Malay (n=126).....	50
Table 5:18	Mean and standard deviation of the perimeter of the right orbit for both races (n=126).....	51
Table 5:19	Comparison of perimeter of the right orbit between the Malay and non-Malay (n=126).....	52
Table 5:20	Mean and standard deviation of the height of the left orbit for both gender (n=126)	53
Table 5:21	Comparison of height of the left orbit between the male and female participants (n=126).....	55
Table 5:22	Mean and standard deviation of the height of the right orbit for both gender (n=126)	55
Table 5:23	Comparison of height of the right orbit between the male and female participants (n=126).....	57
Table 5:24	Mean and standard deviation of the width of the left orbit for both gender (n=126)	57
Table 5:25	Comparison of width of the left orbit between the male and female participants (n=126).....	59
Table 5:26	Mean and standard deviation of the width of the right orbit for both gender (n=126)	59
Table 5:27	Comparison of width of the right orbit between the male and female participants (n=126).....	61
Table 5:28	Mean and standard deviation of the perimeter of the left orbit for both gender (n=126)	62
Table 5:29	Comparison of perimeter of the left orbit between the male and female participants (n=126).....	63
Table 5:30	Mean and standard deviation of the right perimeter of the eyes for both gender (n=126).....	64
Table 5:31	Comparison of perimeter of the right orbit between the male and female participants (n=126).....	65
Table 5:32	Mean and standard deviation of the height of the left orbit for age group (n=126)	66
Table 5:33	Comparison of height of the left orbit between the participants from different age groups (n=126)	69

Table 5:34	Mean and standard deviation of the height of the right orbit for age group (n=126)	70
Table 5:35	Comparison of height of the right orbit between the participants from different age groups (n=126)	74
Table 5:36	Mean and standard deviation of the width of the left orbit of the eyes for age group (n=126).....	74
Table 5:37	Comparison of width of the left orbit between the participants from different age groups (n=126).....	78
Table 5:38	Mean and standard deviation of the width of the right orbit for age group (n=126)	78
Table 5:39	Comparison of width of the right orbit between the participants from different age groups (n=126)	82
Table 5:40	Mean and standard deviation of the perimeter of the left orbit for age group (n=126)	82
Table 5:41	Comparison of perimeter of the left orbit between the participants from different age groups (n=126)	86
Table 5:42	Mean and standard deviation of the perimeter of the right orbit for age group (n=126)	87
Table 5:43	Comparison of perimeter of the right orbit between the participants from different age groups (n=126)	90

CT Based Three-Dimensional Measurement of Adult Orbit in HUSM

LIST OF ABBREVIATIONS, SYMBOLS AND ACRONYMS

3D	Three dimension
ANOVA	Analysis of Variance
CT	Computed tomography
DICOM	Digital Imaging and Communications in Medicine
FBP	Filtered back projection
MRI	Magnetic resonance imaging
OW	Orbital width
OH	Orbital height
OP	Orbital perimeter
PACS	Picture archiving and communication system
TCP/IP	Transmission Control Protocol/Internet Protocol
WW	Window width
WL	Window level

CT Based Three-Dimensional Measurement of Adult Orbit in HUSM

ABSTRACT

Purpose: To correlate the orbital parameters with age, race and gender of the HUSM population for forensic radiology future reference.

Materials and methods: In an institutional review board-approved study, the authors obtained 126 samples referred to HUSM Radiology Department for CT scan of the head. Measurement of the orbital parameters is done on reconstructed 3D images using electronic calipers on workstation screen with the supervision of the supervisor, a senior radiologist with more than 30 years of experience in the Head and Neck imaging. Correlation and regression was used to assess the association between the orbital parameters with patient's age, race and gender.

Results: We were able to obtain 126 patients in which 113 were Malays, 13 were non-Malays, 68 were male and 58 were female. There was a significant correlation between the left and right orbital height (regression line 0.877), orbital width (regression line 0.759) and orbital perimeter (regression line 0.850). There was no significant statistical difference with race correlation and the orbital anthropometry. In terms of correlation with gender, independent t-test showed there was significant statistical difference in the left orbital height (mean difference 0.05), right orbital height (mean difference 0.06) and right orbital perimeter (mean difference 0.16). One way ANOVA showed that in terms of age, there was a significant statistical difference between the left orbital width

(mean difference 0.16), right orbital width (mean difference 0.15) and left orbital perimeter (mean difference 0.43).

Conclusions: This study provided useful baseline anthropometric data that will be of clinical and surgical interest in ophthalmology, oral and maxillofacial surgery in Kelantan. We recommended that anthropologists, clinicians and forensic experts to obtain this data and use them in any way deemed necessary for the quest of research and knowledge.

Ukuran Orbit Orang Dewasa di HUSM Berpandukan CT Skan Tiga Dimensi

Abstrak

Tujuan: Menghubungkan parameter orbit dengan umur, HUSM untuk rujukan radiology forensic kelak.

Bahan dan kaedah: Pengarang mengambil 126 sampel yang dirujuk ke Jabatan Radiologi HUSM di bawah institusi yang disahkan lembaga kajian. Pengukuran parameter orbit dijalankan dengan menggunakan imej 3D ukuran electronic di stesen kerja CT skan di bawah pengawasan penyelia yang berkhidmat sebagai senior radiologist dengan pengalaman 30 tahun dalam bidang pengimejan Kepala dan Leher. Kita mengkaji asosiasi antara parameter orbit dengan umur, bangsa dan jantina pesakit.

Keputusan: Kami berjaya mengumpul data daripada 126 pesakit di mana 113 adalah pesakit Melayu, 13 adalah pesakit bukan Melayu, 68 adalah lelaki dan 58 adalah perempuan. Kami mendapati hubungan ketara antara ketinggian orbit kiri dan kanan (talian regresi 0.877), kelebaran orbit (talian regresi 0.759) dan perimeter orbit (talian regresi 0.850). Dari segi hubungan dengan bangsa, t-test bebas menunjukkan tiada hubungan statistic ketara. Dari segi hubungan jantina, t-test bebas menunjukkan ada hubungan statistic ketara dalam ukuran ketinggian orbit kiri (perbezaan min 0.05), ketinggian orbit kanan (perbezaan min 0.06) dan perimeter orbit kanan (perbezaan min 0.16). Dari segi kategori umur, sejalan ANOVA menunjukkan perbezaan statistic ketara antara

kelebaran orbit kiri (perbezaan min 0.16), kelebaran orbit kanan (perbezaan min 0.15) dan perimeter orbit kiri (perbezaan min 0.43).

Konklusi: Kajian ini memberi garis dasar yang ketara untuk data antropometri yang bakal menjadi data klinikal dan surgical dalam bidang surgery, optalmology, oral dan maxilofasial di Kelantan. Kami mengesyorkan agar anthropologist, pengamal perubatan dan pakar forensic untuk mengambil data ini dan menggunakannya dalam cara yang sesuai dalam pencarian ilmu dan kajian.

CHAPTER 1

INTRODUCTION

Craniofacial measurement is recently a major focus for sex, race or ethnic determination in Forensic study. Understanding anatomical structure, proportion, and mechanical function of the human body and racial variations in ocular anatomy is vital to clinical assessment and treatment of patients (Weaver, Loftis, Tan, Duma, & Stitzel, 2010). Classically, the direct measurement to the orbital width, height and perimeter on the skull provided is thought to be superior (Bolaños, Pérez, Rodríguez, & González, 1998). However, Tomasz Lepich has proven in their study that manual measurements are prone to mistake and a wider range of variability (Lascala, Panella, & Marques, 2014). CT scan would have been a far better choice with its native software allowing the adjustment of the plane of the skull in multiplanar reconstruction prior 3D reformatting of the skull for measurements.

The orbit is a four-sided pyramid with a posterior apex, anterior base and a medially tilted axis. This forms the basis of the human stereoscopic vision and allows for understanding the location of orbital foramina. Our study would be beneficial to compare mean value for HUSM population compared to international data.

In the adult human the average volume of the orbit is 30 ml (Aviv & Casselman, 2005). The height and width of the orbit is noted to differ according to the age group with the size of it increasing with age (Pessa & Chen, 2002). In fact, there is even difference in terms of the interpupillary distance, outer canthal distance and inner canthal distance in African-American males and females compared with same measurements in caucasians (Pivnick, Rivas, Tolley, Smith, & Presbury, 1999). It is also found that between ethnic, the interpupillary distance, palpebral fissure width and eye protrusion vary significantly between African Americans and Caucasians (Barretto & Mathog, 1999).

Prior to the advent of CT scan, there were multiple other studies attempting to measure the orbital width, height and perimeter using other conventional methods. In most studies, external measurements or photographs have been used to measure the surface anatomy of the eye and surrounding facial regions (Bolaños et al., 1998). Most of the orbital dimensions in developing countries have been mainly studied with the use of plain skull radiographs (Ezeuko, Aligwekwe, Udemezue, & Ejimofor, 2007; Igbigbi & Ebite, 2010; Weaver et al., 2010). Human skulls have been used to measure orbital aperture (Pessa & Chen, 2002). These classic measurements are burdened with errors resulting from construction of the applied instruments (objective error) and from experience of the researcher (subjective error) (Farkas, Tompson, Katic, & Forrest, 2002). With the advances in medical imaging, measurement of the orbit can be done with higher accuracy using 3 dimensional (3D) imaging in reconstructed CT scan (Fawehinmi, Ligha, & Chikwu, 2008).

Anthropological analysis of the orbits using classic anthropometric instruments based on width and height measurements as well as orbital index allows for classification of orbits in terms of their shape, yet it has poor clinical application (Lascalea et al., 2014). Orbital index is the ratio of the greatest height of the orbital cavity to its greatest width multiplied by 100 where the width is measured from the dacryon to the farthest point on the opposite border and the height is measured along a line perpendicular to the width (Merriam-Webster, 2015). Computer graphics is a precise method using the latest achievements in digital data recording. In the subject literature there is evidence in favor of efficiency of digital methods in comparison to the classic ones. In the study by Lascalea *et al.* (2014) skulls were measured with classic craniometric methods using a slide caliper (considering 13 parameters), then the crania were scanned using a specific technique of computed tomography (conical beam computed tomography – CBCT). This study confirmed digital efficiency in measuring the external surface of the cranium. Farkas *et al.* (2002) compared the results of anthropometric methods (direct) and cephalometric (indirect). Because of anatomical

properties of the orbital edge, especially of its zygomatic part, it has been admitted that the measurement error may exceed 0.5 mm.

CT scan is chosen as the modality of choice for this study as it is superior to MRI and ultrasound in terms of bone imaging. The scan is faster taking less than 5 minutes compared to standard MRI taking more than 30 minutes. Ultrasound is operator dependant and prone to error. The orbital CT scan measurement is done using the workstation provided along with the native CT machine. Using reproducible methods, the measurement are accurate with no parallax error as per used in conventional measurement method. Armed with this knowledge and basis, we formulated this study based on the pilot study performed by Ashley A Weaver (Weaver et al., 2010). Our main aim is to correlate the measurement of the orbital rim with the age, race and gender of the HUSM population.

The study would have a great impact and benefit to the society. It is believed that differences in eye and orbit anthropometry are thought to affect the response of the eye when subjected to a traumatic impact. Detailed knowledge on the general population orbital anthropometry would assist in developing goggles and protective eye wear. Orbital trauma is common and patients present to a variety of healthcare professionals depending on the type of injury. It is estimated that more than 1.9 million eye injuries occur each year in the United States, and trauma is the second leading cause of visual impairment. Common causes of eye trauma include motor vehicle crashes (Kuhn, Collins, Morris, & Witherspoon, 1994), military operations (Heier, Enzenauer, Wintermeyer, Delaney, & LaPiana, 1993), and ocular impacts with sporting equipment. A protective eye with sufficient protection would generally be able to reduce the rate of injury in these common conditions. Progress during the last decade in reconstructive surgery of the face, using artificial eyeballs in enucleated patients, justifies the necessity of further research in the domain of thorough metric analysis of the orbits pictured in computed tomography (CT) and magnetic resonance (MR)

techniques. The data obtain from the measurement is of great use to determine the sizes and difference in both orbits in the general population. With the objective measurement provided by digital scanning, the factory producing the artificial eyeball would be able to mass produce a size which fits most of the population.

CHAPTER TWO

LITERATURE REVIEW

CHAPTER 2

LITERATURE REVIEW

2.1 Introduction to CT Scan

In 1979, G.N. Hounsfield and A.M. Cormack were awarded the Nobel Prize in medicine for the invention of CT. The superiority of CT scan is that it is an extremely fast and précised examination that required less than 1 minute scanning time for the whole skull to neck scan. It has the ability to study the bony structure which is not well visualized by the MRI scan.

The major disadvantage of the CT scan lies within the fact that patient is exposed to a higher amount of radiation in comparison to the MRI, plain film and ultrasound study.

Native software available within the workstation of HUSM CT scan machine is a good method of collecting data. It allows communication with the PACS (Picture Archiving and Communication System) which provides storage and access to images from multiple imaging modalities (Choplin, Boehme 2nd, & Maynard, 1992). Image can be retrieved instantly at multiple different locations as long as it is within the specified local network coverage of HUSM. This facilitates the researchers to verify and repeat measurement at different places and locations. The data collected will also be backed up in at least 2 main servers in which if the primary server failed, the secondary server will ensure that the data are preserved. The data may also be sent to another researcher for verification should the need arise.

Digital imaging has a standard of imaging which is internationally acceptable. All images are reviewed, reported and measured on DICOM (Digital Imaging and Communication Systems) approved computer system. DICOM is a standard for handling, storing, printing, and transmitting information in medical imaging. It includes a file format definition and a network communications protocol. DICOM files can be

exchanged between two entities that are capable of receiving image and patient data in DICOM format (NEMA, 2015). Such a system will allow an accurate form of measurement despite the measurement being done on different computing system.

Three dimensional scans are acquired with the advent of multislice multidetector CT scan. A high resolution 3D image can only be obtained with higher multislice CT scan (Fayad, Corl, & Fishman, 2009). HUSM is currently using 128 slices CT scan. Prior studies have demonstrated the usefulness of 3D MDCT imaging for evaluation of facial fractures (Remmler, Denny, Gosain, & Subichin, 2000), detection of intraocular and orbital foreign bodies (Zinreich et al., 1986), and assessment of facial asymmetry (Katsumata et al., 2005). It is thus proven that 3D measurement is a reliable and accurate method of assessment of orbital anthropometry. Correlation with the axial and multiplanar reformatted images will also allow the researchers to examine the soft tissue surrounding the periorbital region.

2.2 Reconstruction Algorithm

Image reconstruction in CT is a mathematical process that generates images from X-ray projection data acquired at many different angles around the patient. Reconstructions that improve image quality can be translated into a reduction of radiation dose because images of acceptable quality can be reconstructed at lower dose (Xu, Taguchi, & Tsui, 2010).

Current generation of CT scan has to use an algorithm which is quick to calculate the data in order to process the image fast. With a wide range of HU ranging up to thousands of value, the calculating process is extensive and immense (Thibault, Sauer, Bouman, & Hsieh, 2007).

Methods based on filtered back projection (FBP) are one type of analytical reconstruction that is currently widely used on clinical CT scanners because of their computational efficiency and numerical stability. Iterative reconstruction has many

advantages compared with conventional FBP techniques. It is yielding lower image noise and higher spatial resolution compared with FBP (Ochs & Buckley, 1993). In addition, iterative reconstruction can reduce image artifacts such as beam hardening, windmill, metal artifacts and demonstrated a potential dose reduction of up to 65% (Tessier & Rougier, 1981) compared with FBP-based reconstruction algorithms.

The selection of reconstruction kernel or algorithms should be based on specific clinical applications. For example, smooth kernels are usually used in brain exams or liver tumor assessment to reduce image noise and enhance low contrast detectability. Radiation dose associated with these exams is usually higher than that for other exams due to the intrinsic lower contrast between tissues. On the other hand, sharper kernels are usually used in exams to assess bony structures due to the clinical requirement of better spatial resolution. Lower radiation dose can be used in these exams due to the inherent high contrast of the structures.

2.3 Three Dimensional (3D) Surface Reconstruction Imaging

The steps to produce a diagnostic quality 3D images requires 2 steps namely surface reconstruction and surface display. To shade the surface of the 3D image projected onto the view plane, an intensity is calculated from the component of the unit normal vector parallel to the view direction. The gradient vector of the 3D density function estimates the surface normal direction since the gradient is perpendicular to surfaces of constant density. Gradient shading contributes to the image quality by giving contrast depends on the surface orientation.

Each voxel certex has two possible states; inside or outside the surface. Each possible configuration has an index, calculated by labeling each vertex with one of two colours depending on whether the vertex is inside or outside the surface. Although there are 256 ways to colour eight vertices with two colours, there are only 15 topologically distinct patterns. From there on, multiple patterns are generated as per

interpreted by the computer. Discussion of the pattern is beyond the scope of this study.

2.4 CT Scan Of The Orbit And Brain

In an ideal CT scan of the orbit, the patient is positioned supine with mid centering of the head and neck. The patient is introduced to the CT gantry head first in a supine position. Patient needs to close their eyes while being scanned. Patient needs to be nil by mouth 4 hours prior to the examination. Prior to the start of the scan, the gantry will be positioned to be parallel to the canthomeatal line.

The general protocol includes the usage of topogram to outline the skull and facial bone of the patient. Selection of coverage level of the scan is from the vertex to the cheek prominence on the topogram. Should IV contrast be required, it will be administered at 1mg/kg 300mg/ml via hand injection. The scan will be delayed to 2 minutes upon the commencement of hand injection.

Most of the scans being done were brain study which incidentally includes the orbit as well. The effective mAs for the topogram sequence is 99mAs with the head sequence using 450mAs. The slice thickness will be 1.0mm cut with recon increment of 5.0mm. In this sequence, the orbit will undergo a slice thickness of 5.0mm with recon increment of 5.0mm. An estimated 25 images will be produced using kernel H31s in base orbita window (CTisus, 2015). In general, both pure orbit scan and opportunistic scan of the orbit from a brain will not produce much difference and both are of diagnostic quality.

The CT scan of current 3rd generation are able to complete a full scan within 1 minute and reconstruction will require less than 5 minutes. Compared to the previous 1st and 2nd generation involving rotate-translate and rotate-rotate manner, the current generation is much faster. In the usage of 1st generation CT scan for the brain and orbit scan, the radiographers would have to pre-calculate the distance of the skull and facial

bone coverage and a whole brain scan may take up to 10 minutes requiring the patient to be perfectly stable during the whole scan. 3rd generation CT scan usage in the protocol of brain and orbit scan has advantage of providing thin slice reconstruction and multiplanar reconstruction which was previously not available in the other two earlier generation of CT scan (Bastir, Rosas, & O'Higgins, 2006).

2.5 Anatomy of the Orbit

The orbits are conical structures with the apex located proximally, and the base opens distally onto the facial skeleton. The height of the orbit is usually 35 mm, whereas the width is approximately 40 mm as measured at the rims. From the medial orbital rim to apex, the orbit measures approximately 45 mm in length, whereas from the lateral orbital rim to the apex, the measurement is approximately 1 cm shorter (Ochs & Buckley, 1993; Tessier & Rougier, 1981). The thickened rim is able to resist fracture forces more than the weaker walls, especially the medial wall and floor. Similarly, the thicker bone at the apex shields the brain and the optic nerve from direct force. Pressure to the eye is dispersed to the walls, which absorb the forces and fracture easily.

The orbit is composed of 7 bones. The lateral wall is formed by the greater wing of the sphenoid apically and the frontal and zygomatic bones facially. The floor is formed from the sphenoid, the orbital process of the palatine bone, and the orbital process of the maxillary bone. The medial wall is formed from the lesser wing of the sphenoid, the ethmoid bone, the lacrimal bone, and the frontal process of the maxilla. The roof of the orbit is derived from the sphenoid and the frontal bones (Figure 2.1 & Figure 2.2).

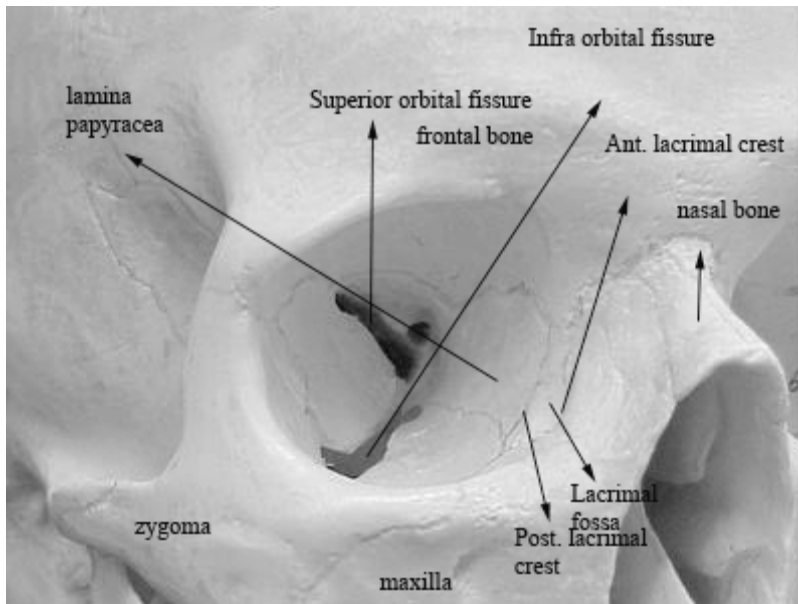


Figure 2.1 Osteology of the orbit (Balasubramanian, 2006)

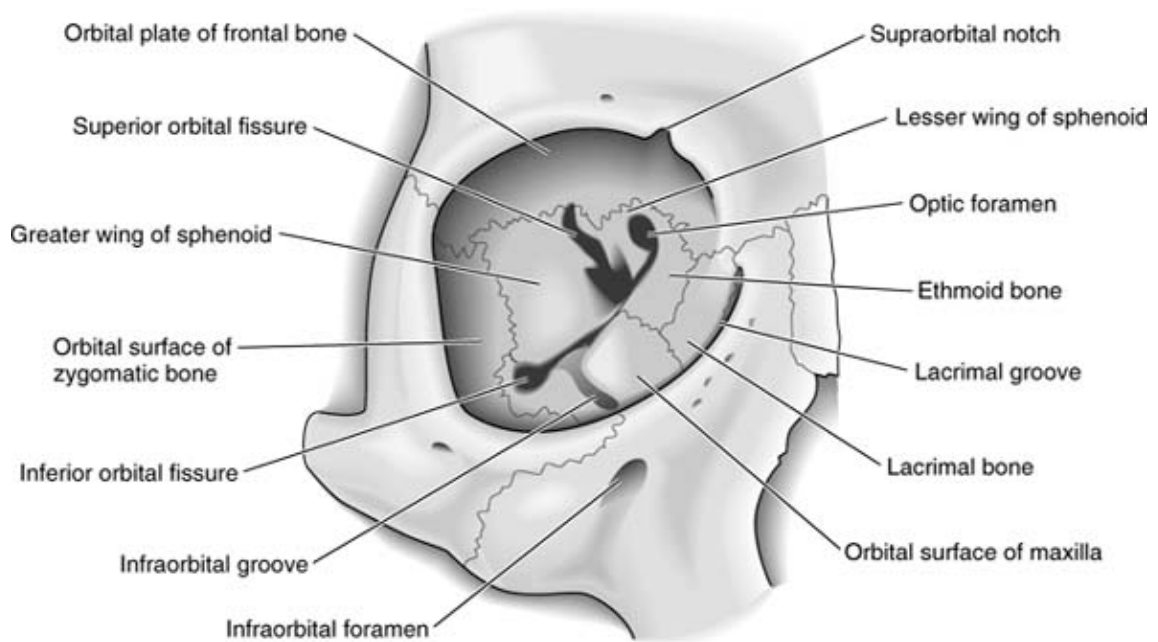


Figure 2.2 Schematic representation of the osteology of the orbit from a frontal projection (John, 2011)

In general, the bone is thickest at the apex, thins as the walls diverge anteriorly, and then thickens again at the rims on the surface of the face. None of the walls of the orbit are flat; they are curvilinear in shape, and their purpose is to maintain the projection of the ocular globe and to cushion it when subjected to blunt force.

From the inferior orbital rim, the floor dips inferiorly while maintaining the same cephalo-caudad position for approximately 15 mm, past the inferior orbital fissure. The medial orbital walls are parallel to the sagittal plane and have the greatest degree of superoinferior curvature. The medial orbital rim is less defined than the other rims. The entire wall is thin from the base to the apex, but it is strengthened by the perpendicular septa of the ethmoid sinus. The wall separates the ethmoid sinuses and nose from the orbit. The roof of the orbit curves cephalically in the lateral aspect to accommodate the lacrimal gland. The bone of this wall separates the anterior cranial fossa from the orbit. It is generally thin and becomes thinner with age. The superior orbital rim has a notch on the medial third through which the supraorbital nerve runs. The lateral orbital rim is the least projected and this facilitates lateral vision. The zygomatic portion of the lateral orbital wall is thin, but the wall thickens considerably in the sphenoid, where it borders the superior orbital fissure.

2.6 Orbital Angle, Fissures and Optic Canal

The arc from medial to lateral wall in each orbit is 45°. Lines dropped through a central anterior-to-posterior axis of each orbit bisect at a 45° angle. The floor is two-thirds the depth of the orbit. The average dimensions of the orbit are as follows with the height of orbital margin at 40 mm, width of orbital margin at 35 mm, depth of orbit at 40-50 mm and interorbital distance at 25 mm (Takahashi et al., 2013).

The major nerves and vessels to the orbit and globe enter via 3 openings. Each openings provide entrance of different structures into the orbit. The superior orbital fissure is bounded by the lesser and greater wings of the sphenoid. The inferior orbital fissure is bounded by the greater wing of the sphenoid, the maxilla, and the palatine bones of the orbit. The optic canal is at the apex of the orbit and lies within the sphenoid bone (Figure 2.3).

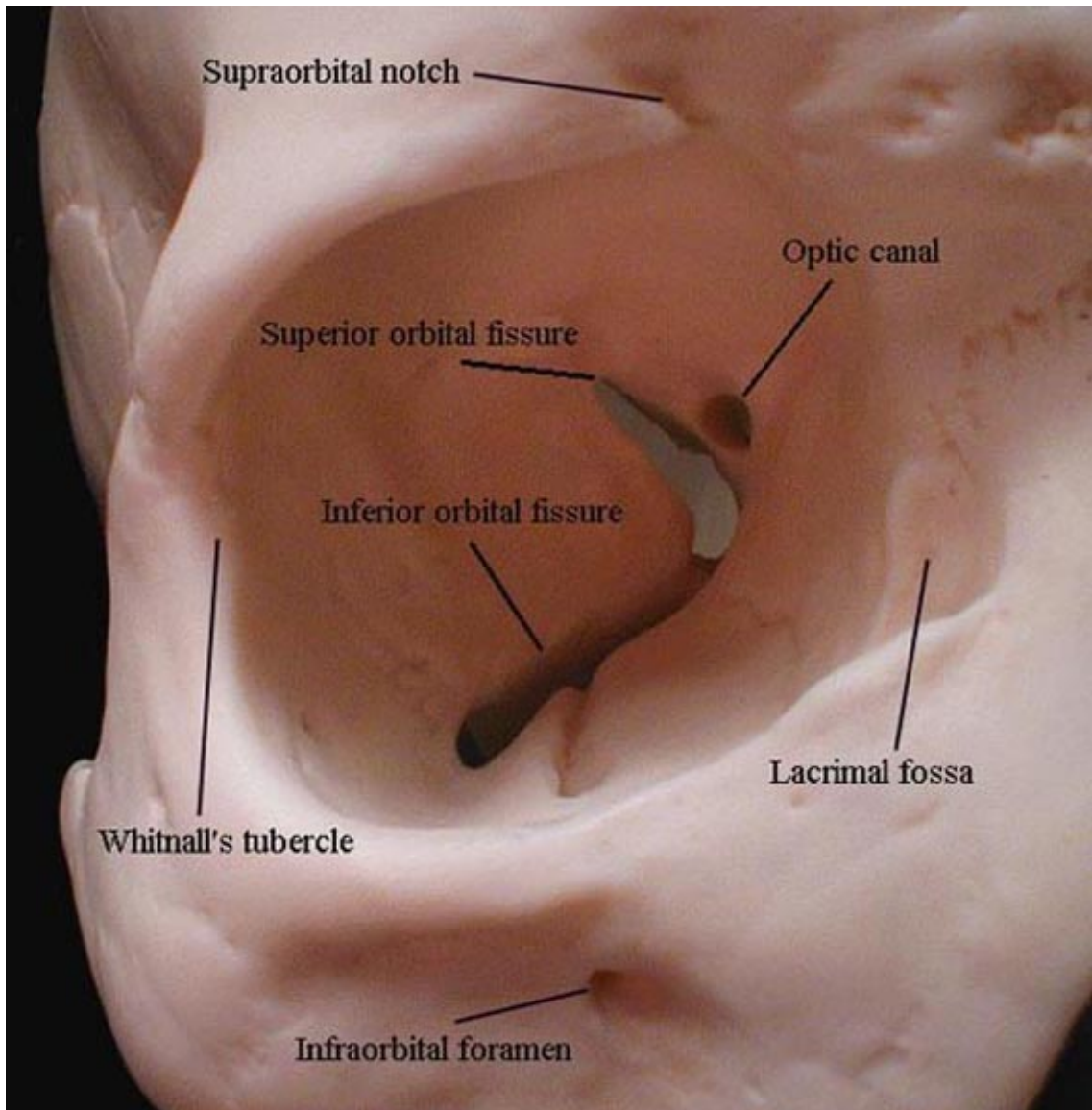


Figure 2.3 Orbital fissure and optic canal (John, 2011)

2.7 Supraorbital Foramina and Infraorbital Foramina

The supraorbital foramen arches transversely below the superciliary arches and is the upper part of the margin of the orbit. It is thin and prominent in its lateral two-thirds, rounded in its medial third. It is the opening for both the supraorbital nerve and vessels

The infraorbital foramen is an opening in the maxillary bone of the skull located below the infraorbital margin. It allows passage for the infraorbital artery, vein, and nerve which are branches of the maxillary branch (V2) of the trigeminal nerve (CN V). The distance between infraorbital foramen and infraorbital margin varies between 6.10 to 10.9 mm. It communicates with the infraorbital groove, the canal's opening on the interior side.

2.8 Extraocular Muscle

There are six muscles (Figure 2.4) that are present in the orbit (eye socket) that attach to the eye to move it. These muscles work to move the eye up and down, side to side, and to rotate the eye. The superior rectus is an extraocular muscle that attaches to the top of the eye. The inferior rectus is a muscle that attaches to the bottom of the eye. The medial rectus is a muscle that attaches to the side of the eye near the nose. The lateral rectus is a muscle that attaches to the side of the eye near the temple. The superior oblique is a muscle that comes from the back of the orbit and travels through the trochlea in the orbit near the nose. It then attaches to the top of the eye. The inferior oblique is a muscle that arises in the front of the orbit near the nose. It then travels outward and backward in the orbit before attaching to the bottom part of the eyeball (Figure 2.5).

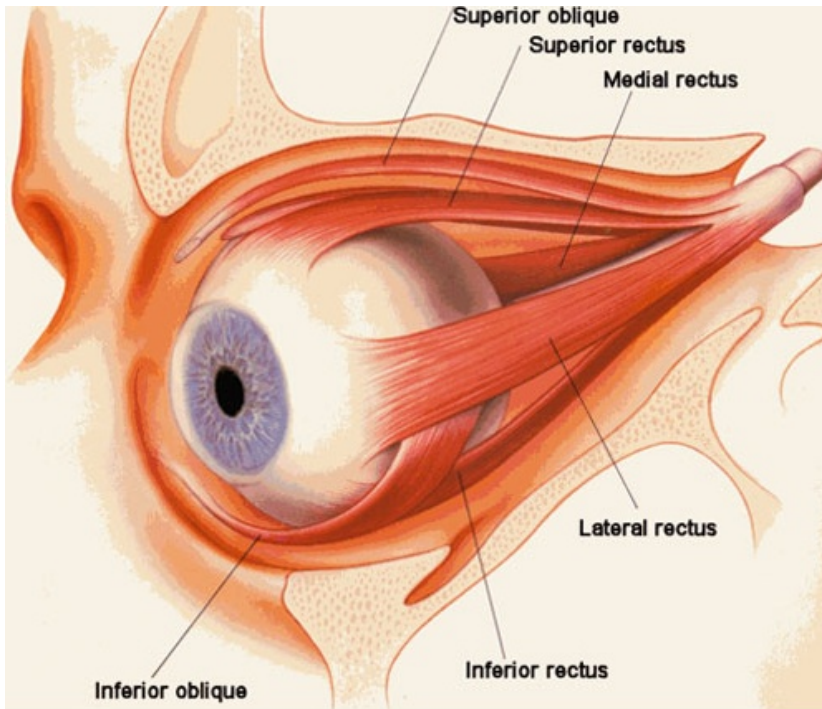


Figure 2.4 Anatomy of the extraocular muscle (AAPOS, 2015)

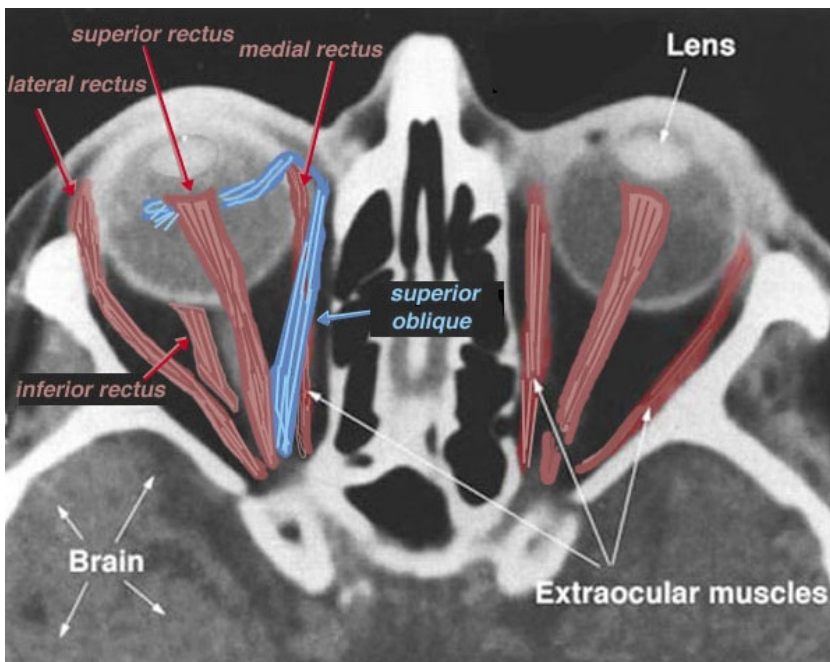


Figure 2.5 Anatomy of extraocular muscle on CT (Kolb, 2015)

2.9 Skull Changes with Age

It has been noted by various researchers that as the age of the patient grows, the skull and hence the orbital size will change with age (Ahmadi, Shams,

Davies, Joshi, & Kelly, 2007). It matures from the base of the skull and subsequently to the face. The changes started from midline cranial base (7–8 years), followed by the lateral cranial floor (11–12 years), midline neurocranium (9–10 years) and facial and mandibular structures (15–16 years).

The skull typically achieves adult morphology by the age of 15.7 years. Different parts of the skull age and achieve adult morphology differently. Although the morphology reached maturity at a fairly young age, another study by H.Ahmadi (2007) showed that as we age, the globe protuberance increased. This is most likely due to a change in the size of the orbit as we age. This is indeed interesting as the combined finding from both studies seemed to suggest that human skull achieves adult morphology early in life but continues to change in size as we age. Minoru Furuta (2001) studied orbital volume using CT scan noted that men and women by age 40 tends to have larger orbital volume which translate to an increment in the orbital anthropometry.

CHAPTER THREE

OBJECTIVES

CHAPTER 3

OBJECTIVE

3.1 General Objectives

To assess the orbit anthropometry based on 3D CT scan in HUSM.

3.2 Specific Objectives

1. To compare the measurement of normalized orbital width, normalized orbital height and normalized orbital rim perimeter of both orbits.
2. To compare the measurement of normalized orbital width, normalized orbital height and normalized orbital rim perimeter with gender.
3. To compare the measurement of normalized orbital width, normalized orbital height and normalized orbital rim perimeter with race.
4. To compare the measurement of normalized orbital width, normalized orbital height and normalized orbital rim perimeter with age group.

CHAPTER FOUR

METHODOLOGY

CHAPTER 4

METHODOLOGY

4.1 Study Design

This prospective study was conducted in Hospital University Sains Malaysia Kubang Kerian from 1st November 2013 till 30th June 2014. This study received ethical approval from Human Research Ethics Committee HUSM. Patients were referred by Accident and Emergency Department, outpatient from Family Medicine Department and in ward patients who developed sudden neurological deficit.

4.2 Research Questions

1. Is there any correlation between the orbital height, width and perimeter with the patient's age, gender and race?
2. Is there any significant difference between the left and right orbital height, width and perimeter of the same patient?
3. What is the sensitivity, specificity, accuracy, positive and negative predictive value, positive and negative likelihood ratio of predicting a person's age, gender and race based on the orbital height, width and perimeter?

4.3 Sampling Method

Sampling method was by purposive sampling.

4.4 Sample Size

We referred to Stats-To-Do website, <http://www.statstodo.com>, to calculate sample size for all our objectives. For all objectives, alpha was determined as 0.05, power of study as 0.8. Sample size was calculated based on Ashley A.Weaver (2010),

using Power and Sample Size (Dupont & Plummer Jr, 2010) total rim parameter as calculation reference.

4.4.1 Sample Size for Objective

We calculated data based on the difference between the male and female gender. The calculated sample size based on normalized orbital width with alpha of 0.17 and standard deviation of 0.14 was 24 patients. The calculated sample size based on normalized orbital height with alpha of 0.15 and standard deviation of 0.15 was 34 patients.

Using the rim perimeter provided in the table given by the author, the alpha value was 2.5 with standard deviation of 5.49, a sample size of 154 was obtained. With these values in mind, a ten percent extra target sample size is obtained in the event that there is incomplete patient data obtained. Thus, the targeted sample size was 169.

4.5 Inclusion criteria

1. Adult patients from 12 years old and above.
2. HUSM population
3. Diagnostic quality image
4. Patient must be conscious throughout the procedure.

4.6 Exclusion criteria

1. Patients with congenital defect of the skull.
2. Patients with previous operation to the skull or orbit.
3. Patients who had trauma to the skull.
4. Patients with carcinoma of orbit or acquired pathology to the orbit.
5. Patients with trauma or acquired pathology which can alter height.

4.7 Methods

All patients who presented to HUSM for CT scan of the brain were screened for fulfillment of inclusion and exclusion criteria. All patients who fulfilled the above screening criteria were asked to give an informed consent. CT scan was performed as per the protocol provided below. The measurements taken were verified randomly by the radiologist who has more than 30 years of experience in reviewing head and neck CT scan.

4.7.1 CT Examination

Most of the patients were either referred from accident and emergency department or in ward patients who developed sudden neurological deficit requiring urgent brain examination to determine the cause.

Prior to the CT scan, patient height was measured based on the following techniques:

1. Using a measuring stick fixed against a wall, we asked patient to stand without shoes with his/her back to the wall and feet against the wall. We would then use the measuring rod on a platform scale.
2. In a supine position, the patient lied on a bed without pillows or wedges. Patient should lie as flat as possible with body and limbs straight. We would then mark the surface at the tip of the head and base of the heels. The length was measured on the flat surface after patient was removed.
3. In arm span measurement technique, using a cloth measuring tape, we asked the patient to extend one arm out. The distance from the sternal notch to the tip of the fingertips was measured and the measurement will be doubled. This distance is to estimate height for potential use in case of patient has difficulty in standing or lying flat.

4.7.2 CT Scan Protocol

The CT scan machine used in HUSM is Siemens SOMATOM Definition AS+ which is capable of producing 128-slices of images per rotation. There were 2 study protocols being utilized.

The first protocol is for CT scan of the orbit and it was used for the patients who were referred for eye and orbit pathology. In CT scan of the orbit, the patient was positioned supine with mid centering of the head and neck. The protocol being used

included the topogram and the orbit with 120kV (kilo Volt) used. The effective mAs (miliAmpere second) used for topogram was 99mAs for the topogram and 125 mAs for the orbit scan. Each slice thickness was 0.75mm with recon increament of 0.5mm. The total images produced were estimated at 101. Kernel applied was H60s produced in the base orbita window.

The second protocol would be opportunistic scan of the brain where in the orbit was included in the study. This protocol differ slightly compared to the CT orbit protocol. It is meant for the imaging of mainly the brain pathology such as cerebrovascular accident and brain tumours. This study would also be using the topogram and the head range in which both use 120kV. The effective mAs for the topogram sequence was 99mAs with the head sequence using 450mAs. The slice thickness was 1.0mm cut with recon increment of 5.0mm. In this sequence, the orbit would undergo a slice thickness of 5.0mm with recon increment of 5.0mm. 25 images were produced using kernel H31s in base orbita window.

4.7.3 Image Analysis

Siemens work station (Siemens Somatom Definition AS+ 128-Slices, dual monitors display utilizing syngo CT 2011A VA40 software) was used for image analysis. The neurology protocol within the work station allowed us to create parallel lines in the vertical and horizontal direction which would be very helpful for measuring the orbital height, width and perimeter.

Image analysis was done on bone window after adjusting to window width of 2200 and window level of 200. Images were adjusted to get proper planes.

We started off adjusting at the sagittal plane. The horizontal grid line was aligned to the base of the skull at the nasion-sella plane. The vertical grid line was then adjusted perpendicular to the horizontal line. The next plane to be adjusted was the axial plane. Using the grid lines provided in the console, the crista galli was aligned to the vertical grid line. Both petrous apex tips were then adjusted until they were at the